JDI Journal of Diabetes Investigation Open access
Official Journal of the Asian Association for the Study of Diabetes
ORIGINAL ARTICLE

YY2 mediates transcriptional repression of PHGDH and expedites oxidative stress in retinal pigment epithelial cells in diabetic retinopathy

Xiang Lei[1], Xiu Wang[2], Xinai Zhang[3]*

[1]Department of Ophthalmology, Henan Eye Institute, Henan Eye Hospital, Henan Provincial People's Hospital, People's Hospital of Zhengzhou University, Zhengzhou, Henan, China, [2]Department of Ophthalmology, Qingdao Municipal Hospital, Qingdao, Shandong, China, and [3]Department of Ophthalmology, Qilu Hospital of Shandong University (Qingdao), Qingdao, Shandong, China

Keywords
Diabetic retinopathy, Ferroptosis, Oxidative stress

***Correspondence**
Xinai Zhang
Tel./Fax: +86-0531-82165391
E-mail address:
zxa028123@qlyyqd.com

J Diabetes Investig 2025; 16: 775–790

doi: 10.1111/jdi.70011

ABSTRACT

Aims/Introduction: Phosphoglycerate dehydrogenase (PHGDH), which controls serine synthesis, has been linked to retinal disease. However, there are no clues about its involvement in the diabetic retinopathy (DR) progression. Therefore, we aimed to investigate the relationship between PHGDH, serine synthesis, and DR and their underlying molecular mechanisms.

Method: Differentially expressed genes in DR were screened using bioinformatics tools. DR mice were induced, and retinal histopathology was observed in mice. Overexpression of PHGDH was induced in the DR mice to measure L-serine, ROS, and MDA content in the retinas of DR mice. ARPE-19 cells were transfected with overexpression of PHGDH and exposed to high glucose to induce a DR *in vitro* model, and cell viability and apoptosis assays, serine content, and oxidative stress factor measurement were conducted. The transcriptional regulation of PHGDH by YY2 was explored by ChIP and dual-luciferase reporter assays. Finally, the combined role of YY2 and PHGDH in regulating serine synthesis, oxidative stress, and ferroptosis was investigated.

Results: PHGDH expression was reduced in DR mice, and overexpression of PHGDH alleviated DR progression by promoting serine synthesis and attenuating oxidative stress. YY2 bound to the promoter of PHGDH and mediated its transcriptional repression. YY2-mediated transcriptional repression of PHGDH caused disturbances in serine synthesis, leading to oxidative stress-triggered ferroptosis.

Conclusions: Our data prove that YY2 plays a vital role in modulating PHGDH expression, impairing serine synthesis, and expediting oxidative stress and ferroptosis.

INTRODUCTION

Diabetic retinopathy (DR), long been recognized as a microvascular disease, is the most common complication of diabetes mellitus[1]. Even though the prevalence of DR is higher in people with T1D (77.3%) relative to T2D (25.2%), both T1D and T2D patients are equally susceptible to DR[2]. DR is a leading contributor to blindness and visual impairment, particularly among working-age adults[3]. The retinal pigment epithelium (RPE), which ensures the normal functioning of the neural retina, is a pigmented single-cell layer that separates the retina from the Bruch's membrane and the choroid[4]. The interaction between RPE cells and microglia affects the integrity of the outer blood-retinal barrier in DR[5]. However, the detailed mechanism has not been fully elucidated.

Phosphoglycerate dehydrogenase (PHGDH), a metabolic enzyme involved in the serine synthesis pathway, has a

Received 6 November 2024; revised 4 February 2025; accepted 10 February 2025

dominant role in promoting cancer growth and proliferation[6]. Interestingly, PHGDH-mediated serine biosynthesis is essential for adipose tissue glucose metabolism and may be a therapeutic target for human diabetes[7]. More relevantly, intracellular ROS and glutathione contents were augmented in primary macular Müller cells which were more susceptible to oxidative stress after suppression of PHGDH[8]. In addition, the loss of serine has been linked to oxidative stress under different contexts[9, 10]. Considering that excessive accumulation of ROS induces mitochondrial damage, cellular apoptosis, lipid peroxidation, and structural and functional changes in the retina[11], we hypothesized that reduction of PHGDH in DR causes serine synthesis impairment, thereby inducing oxidative stress. Yin Yang 2 (YY2) alteration has been recently suggested to negatively regulate the expression of PHGDH and tumor cell *de novo* serine biosynthesis[12]. YY2, a multifunctional zinc finger protein belonging to the YY family, has a dual function in modifying gene expression, acting either as a transcriptional activator or as a repressor of its targets[13]. Its homology YY1 was found to be enhanced in streptozotocin (STZ)-induced diabetic mice and high glucose (HG)-stimulated ARPE-19 cells, and YY1 silencing mitigated HG-induced epithelial-mesenchymal transition and cell permeability[14]. Nevertheless, the role of YY2 in DR has not been well described. Herein, we sought to fill the gap concerning the link between the fine molecular mechanism involved in serine synthesis in DR. To this end, we explored in ARPE-19 cells challenged with HG and mice induced with STZ whether the YY2/PHGDH could be a potential target for counteracting oxidative stress in RPE cells and, subsequently, DR progression.

MATERIALS AND METHODS

STZ-induced DR and intravitreal injection

All experiments were approved by the Institutional Animal Care and Use Committee of Henan Provincial People's Hospital (approval number: KT2023-0531-01; date: 29th, May 2023). C57BL/6J mice (8 weeks, male) were procured from Vital River (Beijing, China) and housed under a 12/12 h light and dark cycle for 1 week, during which they had free access to food and water. The temperature and humidity were controlled.

STZ (HY-13753; MedChemExpress, Monmouth Junction, NJ, USA) (50 mg/kg, solvent 10 mM citrate buffer, pH = 4.5) or an equivalent dose of citrate buffer was injected intraperitoneally into mice for 5 consecutive days[15]. One week after the last injection, blood was harvested from the tail vein to measure the glucose level, and mice with blood glucose levels above 300 mg/dL were deemed successful for modeling. A total of 84 diabetic mice and 12 control mice were successfully generated, and the diabetic mice were allocated into 7 groups. Fundus fluorescein angiography (FFA) was performed on the mice 4 months after diabetes induction, and the mice were subsequently euthanized. Six mice in each group were used for Evans blue staining, and the remaining six were used for other experiments.

Two weeks before diabetes modeling, mice were anesthetized with ketamine at 80 mg/kg and xylazine at 4 mg/kg (*i.p.*), and 1.5 μL of adeno-associated virus (1×10^{12} VG/mL) harboring overexpression of PHGDH and/or overexpression of YY2 plasmids were injected into the vitreous cavity of mice.

Cell culture

Adult retinal pigment epithelial cell line-19 (ARPE-19, catalog number: CL-0026) was cultured in an ARPE-19 specialized medium (catalog number: CM-0026, Dulbecco's modified Eagle's/F12 medium +10% fetal bovine serum +1% penicillin–streptomycin) at 37°C with 5% CO_2 (both from Procell, Wuhan, Hubei, China). Overexpression of PHGDH, overexpression of YY2, knockdown of YY2, and knockdown of PHGDH plasmids were transfected into ARPE-19 cells using Lipofectamine 2000 (11668019; Thermo Fisher Scientific Inc., Waltham, MA, USA). After 48 h of transfection at 37°C with 5% CO_2, the effect of the intervention of the target genes was analyzed using RT-qPCR. Post-transfected cells were treated with HG (25 mM) for 48 h to mimic *in vitro* diabetes, and control cells were cultured in a medium containing normal glucose (control, 5.5 mM). An osmotic control group containing normal glucose (5.5 mM) with 19.5 mM mannose was also set. To explore the relationship between L-serine and oxidative stress, ARPE-19 cells were treated with L-serine (400 μM, HY-N0650; MedChemExpress) or PBS for 6 h.

FFA

Mice were anesthetized with intraperitoneal injections of ketamine (80 mg/kg) and xylazine (10 mg/kg), and 0.125% atropine was dropped on the surface of the eye to dilate the pupil. The mice were injected intraperitoneally with 0.05 mL of 10% sodium fluorescein and examined using a digital fundus camera after 2 min. The fluorescence intensity of the photographs obtained from each group was analyzed by ImageJ software[16].

Hematoxylin–eosin (HE) staining

The mice were euthanized with sodium pentobarbital intraperitoneally (150 mg/kg), and the eyeballs were rapidly harvested and fixed with 4% paraformaldehyde (PFA), paraffin-embedded, and sectioned at 5 μm. A HE staining kit (E607318; Sangon, Shanghai, China) was used. In brief, paraffin-embedded sections were deparaffinized, incubated with drops of hematoxylin staining solution for 5 min at room temperature (RM), treated with 1% hydrochloric acid-ethanol for 30 s, and decolorized in PBS for 60 s. After that, the sections were washed with 95% ethanol for 5 s, counter-stained in eosin staining solution for 2 min, dehydrated in ethanol, sealed with xylene, and placed under the microscope for photographing

and observation. The thickness of the major retinal layers was calculated, including the ganglion cell layer (GCL), inner plexiform layer (IPL), inner nuclear layer (INL), outer plexiform layer (OPL), outer nuclear layer (ONL), photoreceptor layer (PRL), and RPE.

Immunofluorescence staining

Mouse retinal paraffin-embedded sections were dewaxed, hydrated, and placed in 10 mM sodium citrate (pH = 6.0) for heat-induced antigen retrieval. Tissue slides were permeabilized with 1% Triton X-100 for 1 h, sealed with 5% bovine serum albumin for 1 h at room temperature, and incubated overnight at 4°C with Alexa Fluor 647-coupled anti-YY2 (1:100, sc-377008 AF647; Santa Cruz Biotechnology Inc., Santa Cruz, CA, USA) or anti-PHGDH (1:100, ITA2874-647; G-Biosciences, St. Louis, MO, USA). After incubation, slides were stained with DAPI for 5 min at room temperature. Images were acquired using fluorescence microscopy, and the mean fluorescence intensity was quantified by ImageJ.

Retinal trypsin digestion

Mouse eyes were fixed with 4% PFA overnight. The retinas were isolated under a microscope and were digested with 3% trypsin in 0.1 M Tris buffer (pH = 7.8) at 37°C for 1.5 h. The retinas were gently shaken, washed, mounted on slides, stained with Glycogen PAS Staining Kit (G1281; Solarbio, Beijing, China), and observed under a light microscope.

Evans blue assay

Six randomly selected mice from each group were anesthetized by intraperitoneal injection of ketamine (80 mg/kg) and xylazine (4 mg/kg), and Evans blue dye (45 mg/kg) was administrated into the tail vein. The mice were euthanized after 2 h. The thoracic cavity was opened, and the left ventricle was perfused with 0.05 M citrate buffer. The eyeballs were removed and fixed for 30 min at RM in 4% PFA to isolate the mouse retinas. The tissues were imaged under a fluorescence microscope.

Measurements of MDA and ROS contents

MDA content in ARPE-19 cells and retinal tissues was assessed using the MDA Content Assay Kit (BC0025; Solarbio). The cells were transferred and centrifuged to discard the supernatant, added with extraction solution (1×10^5 cells/mL), and subjected to ultrasonication (power 200 W, ultrasonic 3 s, interval 10 s, repeated 30 times). After another centrifugation at 8,000 *g* at 4°C for 10 min, the supernatant was collected for measurement. As for tissue measurement, 1 mL of extraction solution was added into 0.1 g of tissue samples for homogenization on the ice and centrifuged at 8,000 *g* for 10 min at 4°C. The supernatant was harvested for the following assay. Pierce BCA Protein Assay Kit (23225; Thermo Fisher Scientific) was used to quantify proteins. The MDA assay working solution and samples were added. The samples were water-bathed at 100°C for 60 min, and the optical density (OD) value was measured at 532 and 600 nm. MDA content was calculated according to protein concentration.

The working solution was prepared as per the protocol of the ROS Assay Kit (E-BC-K138-F; Elabscience Biotechnology Co., Ltd., Wuhan, Hubei, China) to detect ROS levels in ARPE-19 and retinal tissues. ARPE-19 cells were collected by centrifugation at 1,000 *g* and resuspended in Reagent I working solution at 1×10^5 cells/mL. Tissues were prepared into single-cell suspensions by enzymatic digestion according to the steps in the instructions, and the single-cell suspensions were added to the Reagent I working solution. The cells were incubated at 37°C in darkness for 1 h, centrifuged at 1,000 *g* for 5 min, rinsed with serum-free cell culture medium, resuspended, and loaded for fluorescence intensity assessment.

Cell viability and apoptosis assays

The Annexin V-FITC/PI Apoptosis Kit (E-CK-A211; Elabscience) was used for apoptosis assessment. The cells were centrifuged at 300 *g* for 5 min and resuspended with PBS. The resuspended cells (1×10^5) were centrifuged at 300 *g* for 5 min to discard the supernatant. The cells were resuspended with 500 μL of diluted 1× Annexin V Binding Buffer, incubated with 5 μL of Annexin V-FITC Reagent and 5 μL of PI Reagent at RM in the dark for 20 min, and loaded into the flow cytometer.

Cell viability was determined according to the instructions of CCK-8 (G021-1-1; JianCheng, Nanjing, Jiangsu, China). In brief, 100 μL of ARPE-19 cells (2×10^4 cells/mL) were added to each well of a 96-well plate and incubated at 37°C in an incubator. After 24 h, 10 μL of CCK-8 was supplemented to each well and incubated for 2 h at 37°C with 5% CO_2, and the OD value was read at 450 nm.

RNA extraction and RT-qPCR

Total RNA was extracted from retinal tissues and ARPE-19 cells using TRIzol reagent (15596026; Thermo Fisher). RNA was reverse-transcribed into cDNA by adding RTase, a reverse-transcriptase enzyme, according to the instructions of the TaqMan One-Step RT-qPCR Kit (T2210; Solarbio), which served as a template for PCR amplification. All primers used are listed in Table 1. All data are presented as fold change after normalization to GAPDH.

ChIP

Chromatin was immunoprecipitated using a ChIP Kit (17-295; Merck Millipore, Darmstadt, Germany). The cross-linking of ARPE-19 cells was processed by 1% PFA, which was terminated via glycine. After the cell lysis, the

Table 1 | Primer pairs used for RT-qPCR

Gene	Forward sequence (5′–3′)	Reverse sequence (5′–3′)
PHGDH (human)	CTTACCAGTGCCTTCTCTCCAC	GCTTAGGCAGTTCCCAGCATTC
PHGDH (mouse)	CCTCCTTTGGTGTTCAGCAGCT	CGCACACCTTTCTTGCACTGAG
YY2 (human)	TCCTATGGAGGACATTCCGACG	CTGCAACACCATCAATGGCGGA
YY2 (mouse)	GGAAGCCAGATGGTTTTGCCAG	GCTCACCTTGACCATTCTCTGC
GAPDH (human)	GTCTCCTCTGACTTCAACAGCG	ACCACCCTGTTGCTGTAGCCAA
GAPDH (mouse)	CATCACTGCCACCCAGAAGACTG	ATGCCAGTGAGCTTCCCGTTCAG

GAPDH, glyceraldehyde-3-phosphate dehydrogenase; PHGDH, phosphoglycerate dehydrogenase; YY2, Yin Yang 2.

chromatin was sheared via sonication. The lysates were incubated with the antibodies for YY2 (1:100, sc-374455; Santa Cruz Biotechnology Inc.) or IgG (1:100, sc-3879; Santa Cruz) overnight at 4°C. Precipitation complexes were enriched with protein A agarose, and phenol-chloroform was used to isolate and purify DNA. The PHGDH promoter enrichment was detected by qPCR.

Dual-luciferase report assay

he binding sites (BS) of YY2 on the PHGDH promoter fragment (chr1: 119710728–119713074) were predicted by the Jaspar database (https://jaspar.genereg.net/). Wild-type (WT) PHGDH promoter fragments were generated by PCR from human genomic DNA, and targeted mutagenesis of BS by gene splicing by overlap extension PCR. WT or mutant (MT) PHGDH promoter fragments were inserted into the pGL3-basic plasmid (Promega Corporation, Madison, WI, USA) to construct a luciferase reporter plasmid, followed by transfection of the luciferase reporter plasmid into ARPE-19 cells overexpressing YY2 using Lipofectamine 2000 transfection reagent. After 48 h, luciferase activity was measured with a dual-luciferase reporter assay system (E2920; Promega).

L-serine assay

Determination of L-serine content was performed using the DL-Serine Assay kit (ab241027; Abcam, Cambridge, UK). Retinal tissues were ground to homogenate in ice-cold PBS, and 1×10^6 ARPE-19 cells were resuspended with 100 μL of PBS. Tissue homogenates and cell suspensions were centrifuged for 40 min at 4°C at 15,000 *g*, and supernatants were removed. The sample cleanup mix was supplemented to the sample at 1:25, incubated at 37°C for 15 min, transferred to a 10 kDa MWCO centrifuge column, and centrifuged at 10,000 *g* for 10 min. The processed samples were added to a 96-well plate. For each sample tested, at least three parallel sample wells were prepared: one for the determination of D-serine only, one for the determination of total serine (including both D- and L-isomers), and one to serve as a sample background control. The volume of all wells was adjusted to 60 μL/well with serine assay buffer. The reaction mixture was added and incubated for 60 min at 37°C in darkness, and fluorescence was detected at Ex/Em = 535/587 nm. L-serine content = total serine content − D-serine content.

Iron content testing

Tissue iron content was measured with the Tissue Iron Content Assay Kit (BC4355; Solarbio). Approximately 0.1 g of tissues was added with 1 mL of extraction solution for ice bath homogenization, followed by 4,000 *g* centrifugation at 4°C for 10 min. The supernatant was harvested for sampling, and the OD value was read at 520 nm. The tissue iron content was calculated according to the concentration of tissue protein. The Pierce BCA Protein Assay Kit (23225; Thermo Fisher) was used to quantify proteins.

The iron content in the cells was determined by the Cellular Iron Content Assay Kit (BC5310; Solarbio). In brief, 10^4 cells were added with the extraction solution and ultrasonically broken. The samples were added according to the instructions, and the color was developed at 25°C for 10 min. The OD

Figure 1 | PHGDH is significantly reduced in retinal tissues of mice with DR and ARPE-19 cells induced with HG. (a) A total of 618 DEGs were screened in the GSE233164 dataset using GEO2R with Benjamini & Hochberg corrected *P*-value, threshold adj. *P* value <0.05, LogFC >2. (b) The intersection of DEGs in the GSE233164 dataset with genes associated with DR. (c) Differential expression of PHGDH in the GSE233164 database ($n = 3$). (d) The retinal vascular changes in mice after STZ induction were analyzed using FFA ($n = 12$). (e) Changes in the number of pericyte ghosts, cell-free capillaries, and microaneurysms in mouse retinal tissues after STZ induction detected by trypsin digestion ($n = 6$). (f) Changes in retinal tissue thickness after STZ induction were observed by HE staining ($n = 6$). (g) Retinal vascular leakage in mice was observed using Evans blue staining ($n = 6$). (h) Detection of PHGDH mRNA levels in retinal tissues of DR mice by RT-qPCR ($n = 6$). (i) Detection of PHGDH protein levels in retinal tissues of DR mice by immunofluorescence staining. Data are expressed as mean ± SD. $^*P < 0.05$. The statistical test used in (d, e, g–i) is the unpaired *t*-test, and in (f) is a two-way ANOVA.

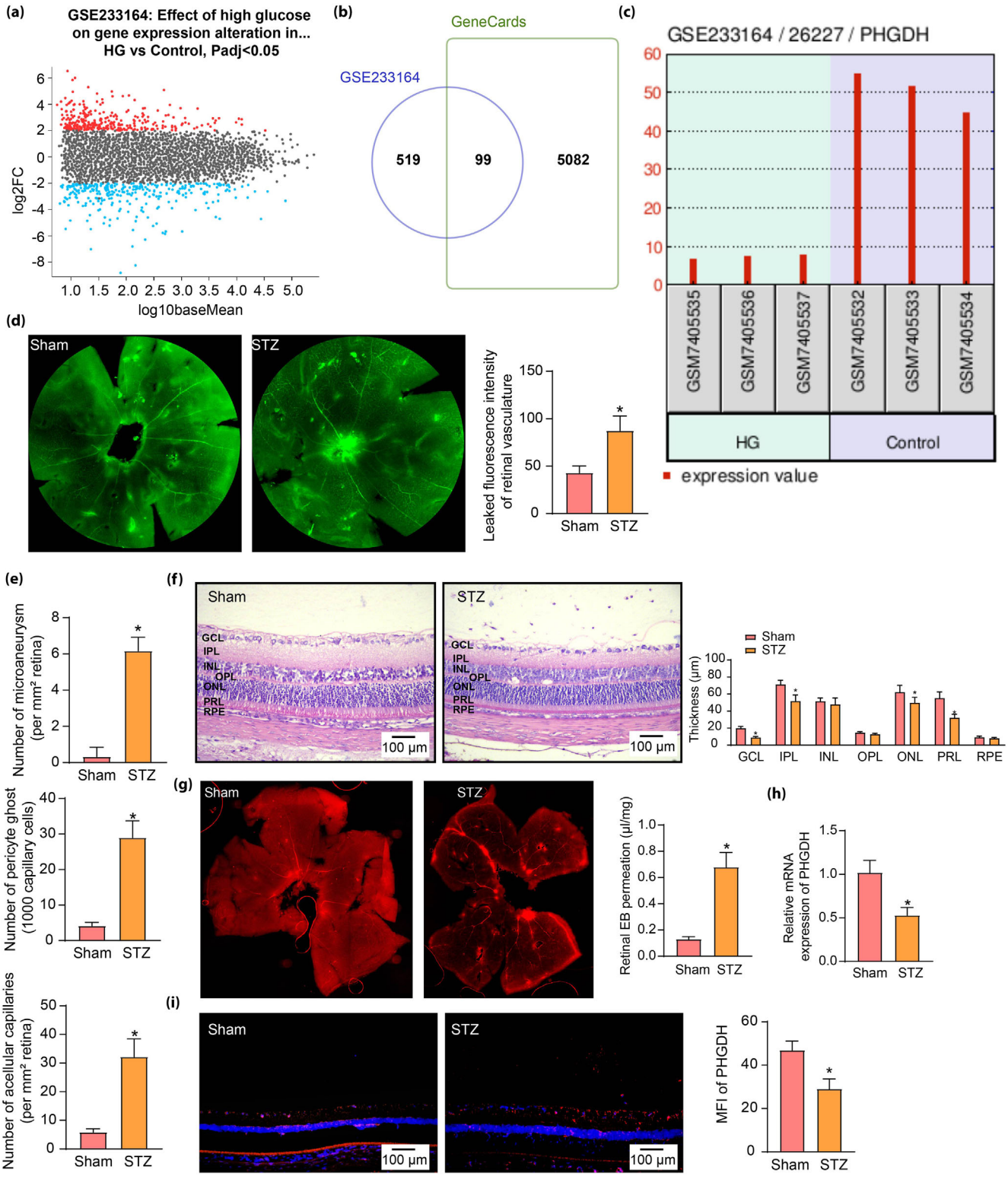
(a)
GSE233164: Effect of high glucose on gene expression alteration in... HG vs Control, Padj<0.05
log2FC
log10baseMean
(b)
GeneCards
GSE233164
519
99
5082
(c)
GSE233164 / 26227 / PHGDH
GSM7405535
GSM7405536
GSM7405537
GSM7405532
GSM7405533
GSM7405534
HG
Control
expression value
(d)
Sham
STZ
Leaked fluorescence intensity of retinal vasculature
(e)
Number of microaneurysm (per mm² retina)
Number of pericyte ghost (1000 capillary cells)
Number of acellular capillaries (per mm² retina)
(f)
GCL
IPL
INL
OPL
ONL
PRL
RPE
100 μm
Thickness (μm)
(g)
(h)
Retinal EB permeation (μl/mg)
Relative mRNA expression of PHGDH
(i)
MFI of PHGDH

value at 510 nm was measured, and the cellular iron content was evaluated according to the number of cells.

Western blot analysis

Retinal tissues or ARPE-19 cells were lysed using RIPA lysis buffer, and proteins were quantified with the Pierce BCA Protein Assay Kit (23225; Thermo Fisher). Proteins were separated by 10% SDS-PAGE and transferred to PVDF membranes. The membranes were sealed with 4% skimmed milk and 0.1% Tween-20 and probed with primary antibodies to SLC7A11 (1:1,000, NB300-318SS; Novus Biological Inc., Littleton, CO, USA), GPX4 (1:1,000, ab125066; Abcam), and β-actin (1:200, ab8227; Abcam) overnight at 4°C and with the HRP-conjugated secondary antibody (1:2,000, ab6721; Abcam) at RM for 2 h. The membranes were visualized using ECL Substrate and analyzed using ImageJ.

Statistics

All data represent the mean ± SD. GraphPad Prism 10.4.1 software (GraphPad, San Diego, CA, USA) was used for statistical analyses. The difference was compared by unpaired *t*-test for two groups by ANOVA followed by Tukey's or Šídák's post hoc test for multiple groups. A *P*-value less than 0.05 was considered statistically significant.

RESULTS

PHGDH is significantly downregulated in retinal tissues in DR mice

We downloaded the gene expression profiling analysis of mRNA-sequencing and long noncoding RNA sequencing data for ARPE-19 cells at normal and HG media for 72 h from the GSE233164 database (https://www.ncbi.nlm.nih.gov/geo/query/acc.cgi?acc=GSE233164). By using GEO2R with Benjamini & Hochberg corrected *P*-value, setting adj. *P*. value <0.05 and LogFC >2 as the threshold, we screened a total of 618 differentially expressed genes (DEGs) (Figure 1a). Genes related to DR according to the keyword "diabetic retinopathy" were downloaded from GeneCards database (https://www.genecards.org/), followed by intersection with the DEGs. The results showed that there were 99 intersected genes (Figure 1b). Further analysis of the differential expression of the intersecting genes in the ARPE-19 cells after HG treatment revealed that PHGDH was the most significantly differentially expressed gene (adj. *P* value = 1.65E-110) and its expression was reduced in ARPE-19 cells induced with HG (LogFC = –2.82792106, Figure 1c). Therefore, we established a DR animal model to further validate the role of PHGDH in DR.

Retinal vascular changes in mice were detected by FFA, which showed a significant promotion in fluorescence leakage from microvessels and retinal microangioma formation in the STZ-treated mice relative to the sham-operated mice (Figure 1d). Trypsin digestion of the retina was performed to detect the number of microaneurysms, pericyte ghost, and acellular capillaries. STZ induction increased the number of microaneurysms, pericyte ghost, and acellular capillaries in the mouse retina (Figure 1e). Reduced retinal thickness (including GCL, IPL, ONL, and PRL) was observed in STZ-treated mice using HE staining (Figure 1f). Evans blue staining showed increased retinal vascular leakage in mice by STZ treatment (Figure 1g). Finally, RT-qPCR was carried out and confirmed that PHGDH mRNA levels were reduced in DR mice (Figure 1h). Immunofluorescence staining observed that PHGDH in the mouse retina was predominantly expressed in the RPE. DR modeling resulted in a significant loss of PHGDH expression (Figure 1i).

Overexpression of PHGDH alleviates DR progression in mice induced with STZ

To investigate the effect of overexpression of PHGDH on DR, we infected mice with adeno-associated virus-harboring overexpression of PHGDH plasmid and induced mice with STZ. First, we observed retinal vascular changes in mice with FFA, and injection of OE-PHGDH alleviated fluorescence leakage and retinal microangioma formation in mouse microvessels (Figure 2a). Then, we verified that overexpression of PHGDH was effective by detecting PHGDH mRNA levels with RT-qPCR (Figure 2b). Overexpression of PHGDH reduced the number of pericyte ghosts, acellular capillaries, and microaneurysms in the retinas of DR mice, as detected by trypsin digestion of the retina (Figure 2c). HE staining observations revealed that

Figure 2 | Ectopic expression of PHGDH relieves DR in mice induced with STZ. Mice were infected with adeno-associated virus-encapsulated overexpression PHGDH plasmid and induced with STZ. (a) The retinal vascular changes in mice after overexpression of PHGDH were analyzed using FFA (n = 12). (b) The expression of PHGDH in the retinal tissues of DR mice was determined using RT-qPCR (n = 6). (c) The number of pericyte ghosts, acellular capillaries, and microaneurysms in mouse retinal tissues after STZ induction was detected by trypsin digestion (n = 6). (d) Changes in retinal tissue thickness after STZ induction were observed by HE staining (n = 6). (e) Retinal vascular leakage in mice was observed using Evans blue staining (n = 6). Data are expressed as mean ± SD. *P < 0.05. The statistical test used in (a–c, e) is an unpaired *t*-test, and in (d) is a two-way ANOVA.

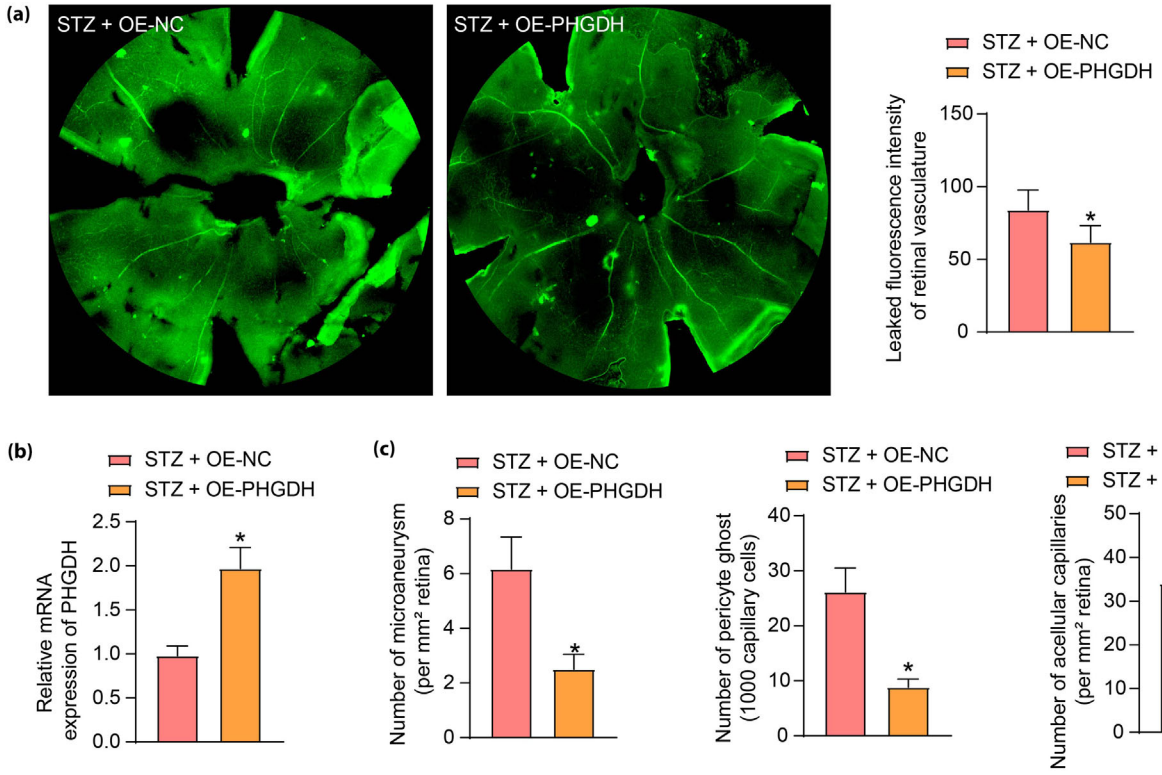
(a)
STZ + OE-NC
STZ + OE-PHGDH
Leaked fluorescence intensity of retinal vasculature
150
100
50
0
*
(b)
Relative mRNA expression of PHGDH
2.5
2.0
1.5
1.0
0.5
0.0
(c)
Number of microaneurysm (per mm² retina)
8
6
4
2
0
Number of pericyte ghost (1000 capillary cells)
40
30
20
10
0
Number of acellular capillaries (per mm² retina)
50
40
30
20
10
0
(d)
GCL
IPL
INL
OPL
ONL
PRL
RPE
100 μm
Thickness (μm)
80
60
40
20
0
(e)
Retinal EB permeation (μl/mg)
1.0
0.8
0.6
0.4
0.2
0.0

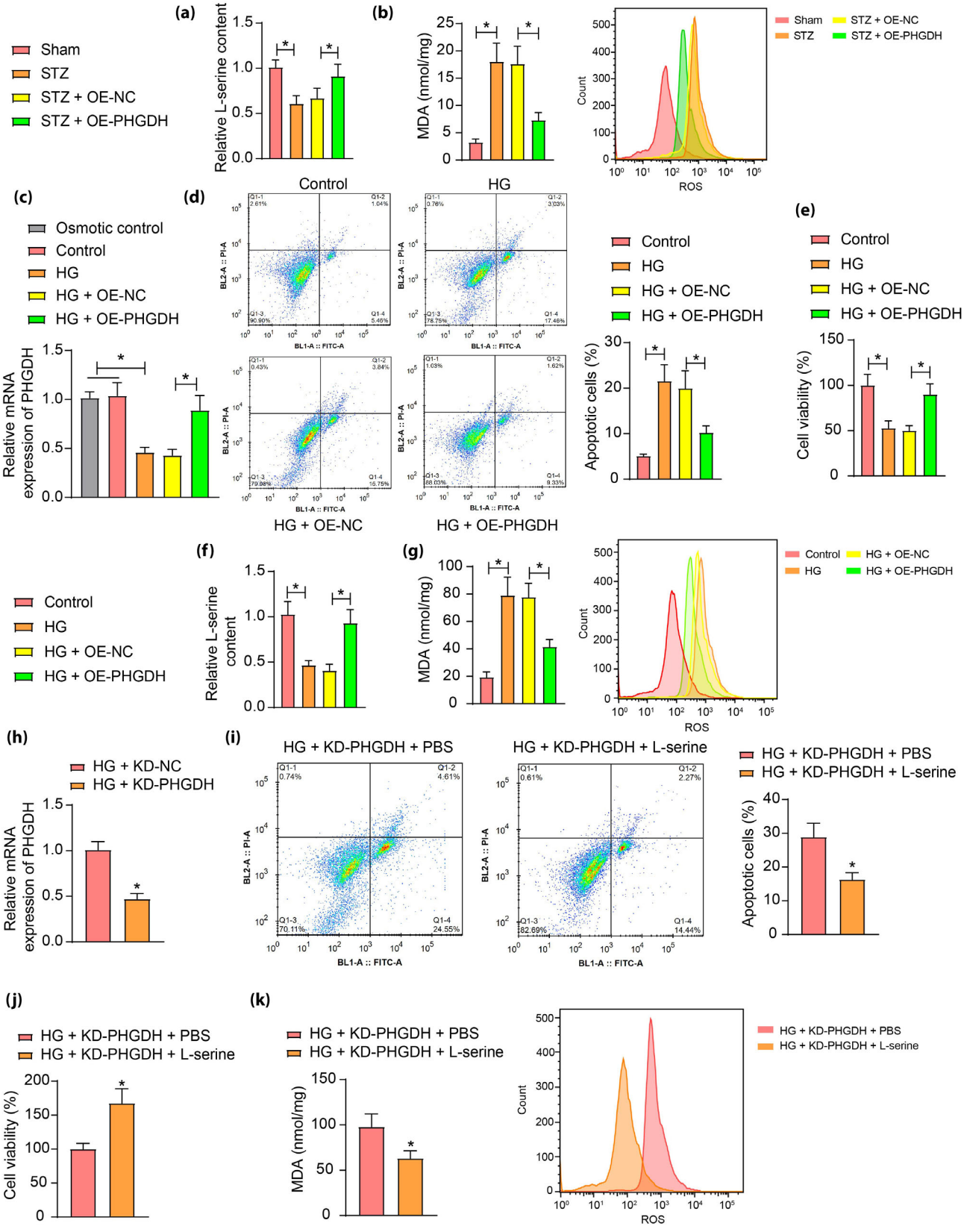

Figure 3 | Overexpression of PHGDH promotes serine synthesis and alleviates oxidative stress in DR mice and ARPE-19 cells induced with HG. (a) L-serine content in mouse retina in response to STZ treatment and overexpression of PHGDH ($n = 6$). (b) Detection of the effects of STZ treatment and overexpression of PHGDH on MDA and ROS content in mouse retinal tissues ($n = 6$). ARPE-19 cells were transfected with overexpression of PHGDH plasmid and induced with HG to establish a DR cell model. (c) The expression of PHGDH in the ARPE-19 cells after transfection was determined using RT-qPCR ($n = 3$). (d) Changes in apoptosis of ARPE-19 cells detected by flow cytometry ($n = 3$). (e) Cell viability after overexpression of PHGDH and HG induction in ARPE-19 cells was measured using CCK-8 ($n = 3$). (f) Effect of overexpression of PHGDH and HG induction on serine content in ARPE-19 cells ($n = 3$). (g) Effects of overexpression of PHGDH and HG induction on MDA and ROS content in ARPE-19 cells ($n = 3$). ARPE-19 cells were transfected with knockdown of PHGDH plasmid and induced with HG. (h) The expression of PHGDH in the ARPE-19 cells after transfection was determined using RT-qPCR ($n = 3$). (i) The effect of L-serine on apoptosis of ARPE-19 cells with PHGDH knockdown was measured using flow cytometry ($n = 3$). (j) Effect of L-serine on cell viability of ARPE-19 cells with PHGDH knockdown measured using CCK-8 assay ($n = 3$). (k) Effect of L-serine on MDA and ROS content in ARPE-19 cells with PHGDH knockdown ($n = 3$). Data are expressed as mean ± SD. $^*P < 0.05$. The statistical test used in (h–k) is an unpaired *t*-test, and in (a–g) is a one-way ANOVA.

overexpression of PHGDH increased the thickness of GCL, IPL, ONL, and PRL in the retina of DR mice (Figure 2d). The representative images of Evans blue staining in Figure 2e showed that overexpression of PHGDH alleviated retinal vascular leakage in DR mice.

Overexpression of PHGDH promotes serine synthesis and attenuates oxidative stress

To examine the relationship between PHGDH and serine synthesis and oxidative stress, we first detected changes in serine content in mice after overexpression of PHGDH. STZ induction decreased L-serine content in the retina of the mice. In contrast, overexpression of PHGDH increased L-serine content in DR mice (Figure 3a). We examined MDA and ROS content in retinal tissues. STZ treatment increased oxidative stress factor levels, whereas overexpression of PHGDH decreased MDA and ROS content (Figure 3b).

Then, we transfected ARPE-19 cells using overexpression of PHGDH plasmid and had them induced with HG to establish a DR cell model. RT-qPCR results showed that HG treatment decreased PHGDH expression in ARPE-19 cells, which was not related to changes in the osmotic pressure of the cells. OE-PHGDH effectively rescued PHGDH expression inhibited by HG (Figure 3c). Cell apoptosis and viability were detected by flow cytometry and CCK-8. HG treatment decreased cell viability and increased the number of apoptotic cells, which was overturned by overexpression of PHGDH (Figure 3d,e). By detecting changes in serine content in cells, we found that HG induction reduced serine synthesis in cells. Overexpression of PHGDH promoted serine synthesis (Figure 3f). Detection of MDA and ROS content in cells to assess oxidative stress status showed an increase in MDA and ROS content after HG induction and a decrease in these factors after overexpression of PHGDH (Figure 3g).

To demonstrate that the serine increase could alleviate the cellular oxidative stress state, ARPE-19 cells with knockdown of PHGDH were first constructed, followed by HG induction. RT-qPCR verified that the knockdown of PHGDH was effective (Figure 3h). Subsequently, these cells were treated with L-serine or PBS. Flow cytometry and CCK-8 assay revealed that L-serine treatment promoted cell viability and decreased apoptosis (Figure 3i,j). The MDA and ROS content in the cells was detected and found to be reduced after L-serine treatment (Figure 3k).

YY2 inhibits the transcription of PHGDH

In the Jaspar database (https://jaspar.genereg.net/), we found multiple binding sites for YY2 on the PHGDH promoter based on the PHGDH promoter sequence (Figure S1A,B). In the ChIP-seq database (http://cistrome.org/db/#/), a binding peak of YY2 on the PHGDH promoter was observed (Figure S1C).

As demonstrated by ChIP, YY2 bound to the PHGDH promoter, which was more pronounced under the exposure to HG (Figure 4a). The mRNA expression of YY2 was enhanced in the DR mice and ARPE-19 cells induced with HG (Figure 4b). Immunofluorescence staining observed YY2 was mainly localized in the RPE and the PRL of mice, and DR modeling resulted in a significant increase in YY2 expression (Figure 4c).

ARPE-19 cells overexpressing YY2 were constructed, and RT-qPCR confirmed that the overexpression of YY2 was effective (Figure 4d). A single BS mutant (MT) PHGDH promoter sequence was designed to construct the corresponding luciferase reporter vector based on the seven BS present in the PHGDH promoter for YY2 (Figure 4e). A total of two sites affecting the transcriptional regulatory role of YY2 were detected by dual-luciferase assays, BS2 (1,367–1,377 bp) and BS3 (1,417–1,427 bp). Mutations in the two sites led to a weakening of the transcriptional repression of the PHGDH promoter by YY2 (Figure 4f). We examined the effects of YY2 knockdown on PHGDH and L-serine under normal and HG conditions and observed that YY2 knockdown significantly increased PHGDH expression and L-serine production in both conditions (Figure 4g,h).

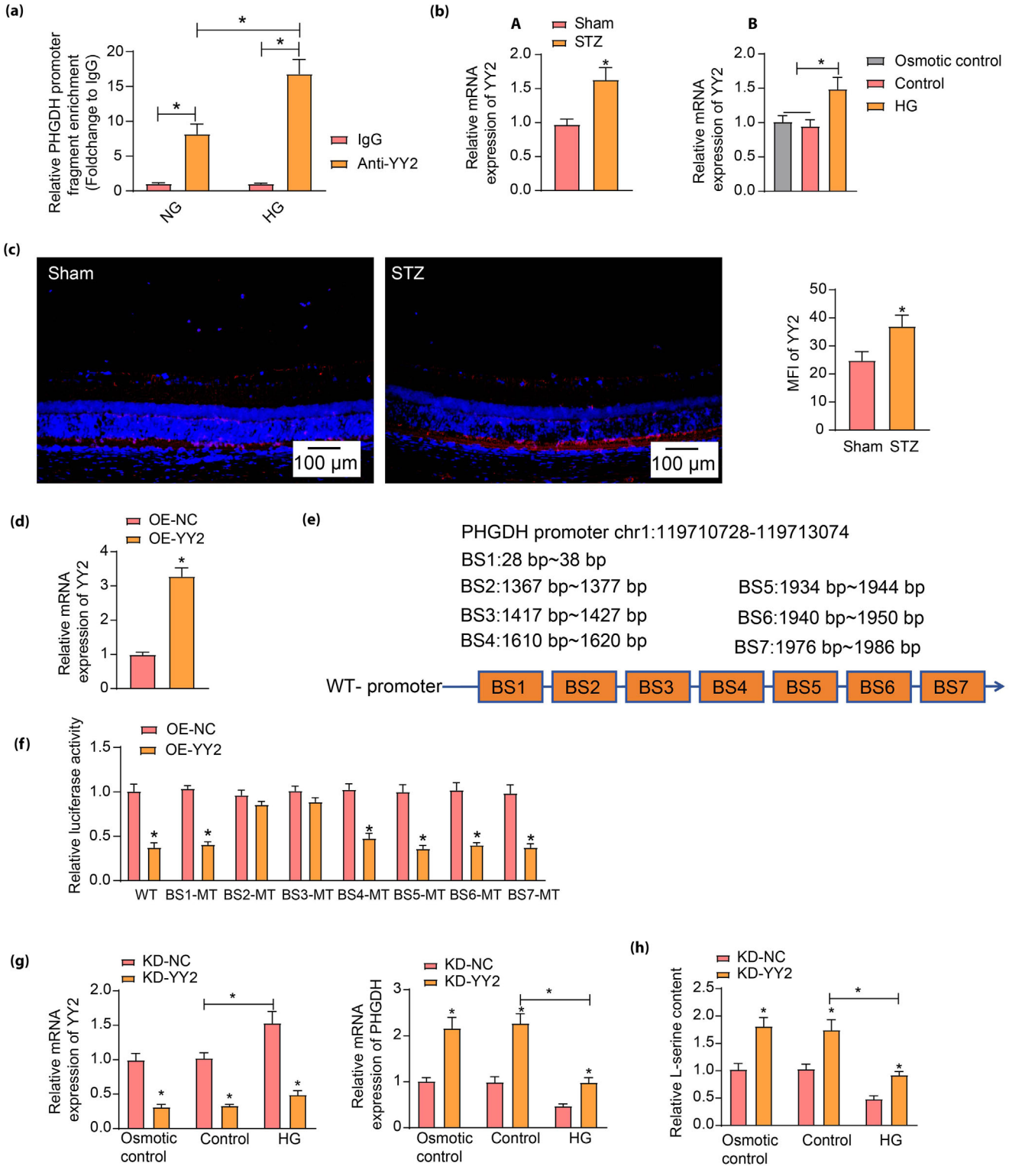

Figure 4 | YY2 mediates transcriptional repression of PHGDH. (a) The binding between YY2 and the PHGDH promoter was verified using ChIP (n = 3). (b) Expression of YY2 in DR mice (n = 6) and cellular models (n = 3) was measured using RT-qPCR. (c) Detection of YY2 protein levels in retinal tissues of DR mice (n = 6) by immunofluorescence staining. ARPE-19 cells were transfected with YY2 overexpression plasmid and induced with HG. (d) The expression of YY2 in ARPE-19 cells was measured using RT-qPCR (n = 3). (e) Seven potential BSs for YY2 binding on the PHGDH promoter. (f) The effect of YY2 on the PHGDH promoter transcription was measured using dual-luciferase reporter assays (n = 3). (g) Effect of knockdown of YY2 on PHGDH expression in ARPE-19 cells detected by RT-qPCR (n = 3). (h) Effect of knockdown of YY2 on serine content in ARPE-19 cells (n = 3). Data are expressed as mean ± SD. *P < 0.05. The statistical test used in (bA, c, d) is the unpaired t-test, in (bB) is a one-way ANOVA, and in (a, f–h) is a two-way ANOVA.

YY2 induces disruption of serine synthesis and oxidative stress-mediated ferroptosis via PHGDH

We overexpressed PHGDH on top of overexpression of YY2 to investigate whether YY2 could disrupt serine synthesis and oxidative stress-mediated ferroptosis by inhibiting the transcription of PHGDH. ARPE-19 cells that had overexpressed YY2 were treated with PHGDH overexpression plasmids and cultured in an HG environment. YY2 overexpression reduced the mRNA expression of PHGDH, while OE-PHGDH was found to upregulate the expression of PHGDH without alteration of YY2 expression, as revealed by RT-qPCR (Figure 5a,b). Increased apoptosis and decreased cell viability after overexpression of YY2 were found by flow cytometry and CCK-8 assay, which was reversed after overexpression of PHGDH (Figure 5c,d). L-serine content was detected. OE-YY2 treatment decreased L-serine content in the cells, and overexpression of PHGDH increased L-serine content (Figure 5e). Enforced expression of YY2 increased MDA and ROS levels, while overexpression of PHGDH alleviated oxidative stress (Figure 5f). Next, the iron content in the cells was detected. The iron content in ARPE-19 cells was elevated after HG treatment, and overexpression of YY2 further increased the iron content in the cells. Overexpression of PHGDH, however, reduced the iron content in ARPE-19 cells (Figure 5g). Finally, the expression of ferroptosis-related proteins in cells was examined by western blot analysis. The protein levels of SLC7A11 and GPX4 were reduced in ARPE-19 cells under HG culture conditions, which was further downregulated after overexpression of YY2. Still, the expression of related proteins was increased by overexpression of PHGDH (Figure 5h).

PHGDH upregulation rescues the accentuating effects of YY2 on DR in mice

We constructed mice overexpressing both YY2 and PHGDH using an adeno-associated virus and induced diabetes with STZ. Retinal vascular changes in mice were observed by FFA, and overexpression of YY2 exacerbated fluorescence leakage from microvessels and retinal microangioma formation, which was alleviated by overexpression of PHGDH (Figure 6a). We detected YY2 mRNA levels in retinal tissues by RT-qPCR and verified that overexpression of YY2 was effective (Figure 6b). Next, trypsin digestion of the retina was performed. Overexpression of YY2 increased the number of pericyte ghosts, cell-free capillaries, and microaneurysms in the retinas of DR mice, which were reversed by overexpression of PHGDH treatment (Figure 6c). HE staining observation revealed that overexpression of YY2 significantly decreased the thickness of IPL, ONL, and PRL in DR mice, which were restored after overexpression of PHGDH (Figure 6d). Overexpression of YY2 also exacerbated retinal vascular leakage in DR mice, while overexpression of PHGDH alleviated retinal vascular leakage (Figure 6e). Serine synthesis was blocked after overexpression of YY2, while overexpression of PHGDH promoted serine synthesis (Figure 6f). MDA and ROS levels were assessed in the tissues. Overexpression of YY2 increased MDA and ROS levels, and oxidative stress was alleviated by PHGDH upregulation (Figure 6g). Moreover, the iron content in the tissues was elevated after overexpression of YY2 and decreased after overexpression of PHGDH (Figure 6h). Finally, ferroptosis-related proteins were detected. YY2 upregulation decreased the expression of both SLC7A11 and GPX4, and PHGDH upregulation increased the expression of ferroptosis-related proteins (Figure 6i).

DISCUSSION

Despite cutting-edge research, molecular events resulting in the development of DR remain unclear[17]. Lowering oxidative stress appears to be an early therapeutic strategy for the diabetes-induced degeneration of the retinal neurovascular unit[18]. Therefore, identifying new pathways that relate to oxidative stress in DR is crucial for improving vision in diabetic patients in the future. Specifically, the role of oxidative stress and its molecular mechanism related to PHGDH expression in the development of DR is the focus of our study.

Hyperglycemia leads to the development of microangiopathy, including microaneurysms, hemorrhages, and basement membrane thickening, resulting in increased vascular permeability of the blood-retinal barrier[19]. Here, we observed the downregulation of PHGDH in the retina of mice exhibiting microaneurysms, pericyte ghosts, and acellular capillaries. These pathological changes were alleviated by PHGDH overexpression using intravitreal injection of adeno-associated virus.

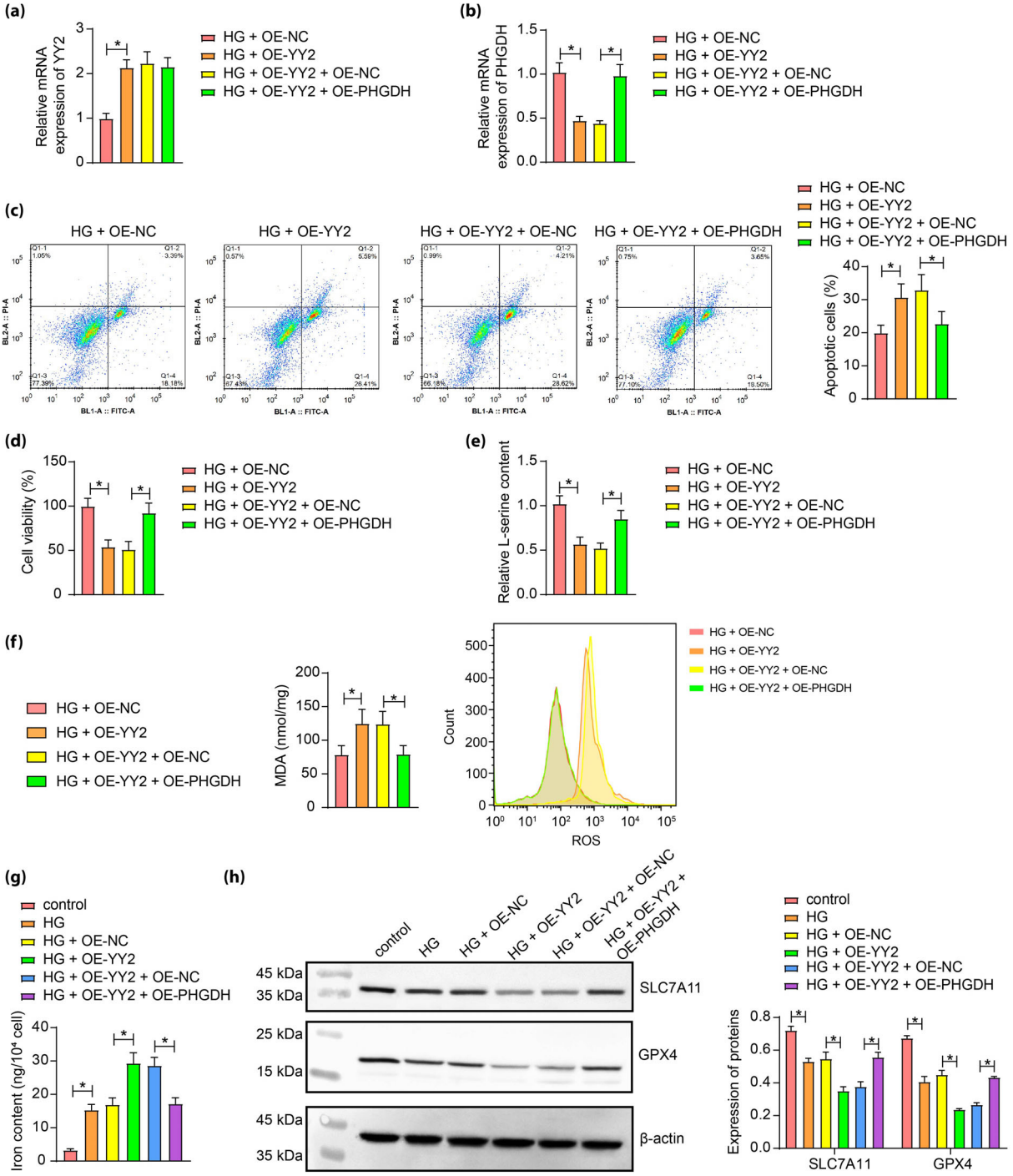

Figure 5 | YY2-mediated transcriptional repression of PHGDH induces disruption of serine synthesis and oxidative stress-triggered ferroptosis. ARPE-19 cells were treated with OE-YY2 alone or in combination with OE-PHGDH. (a) The expression of YY2 in ARPE-19 cells was measured using RT-qPCR (n = 3). (b) Effect of overexpression of YY2 on PHGDH mRNA expression measured using RT-qPCR (n = 3). (c) Changes in apoptosis of ARPE-19 cells detected by flow cytometry (n = 3). (d) Cell viability after overexpression of both YY2 and PHGDH in ARPE-19 cells was measured using CCK-8 (n = 3). (e) Effect of overexpression of both YY2 and PHGDH on serine content in ARPE-19 cells (n = 3). (f) Effects of overexpression of both YY2 and PHGDH on MDA and ROS content in ARPE-19 cells (n = 3). (g) Effects of overexpression of both YY2 and PHGDH on iron content in ARPE-19 cells (n = 3). (h) Effects of overexpression of both YY2 and PHGDH on the expression of ferroptosis-related proteins in ARPE-19 cells (n = 3). Data are expressed as mean ± SD. *P < 0.05. The statistical test used in (a–g) is one-way ANOVA, and in (h) is two-way ANOVA.

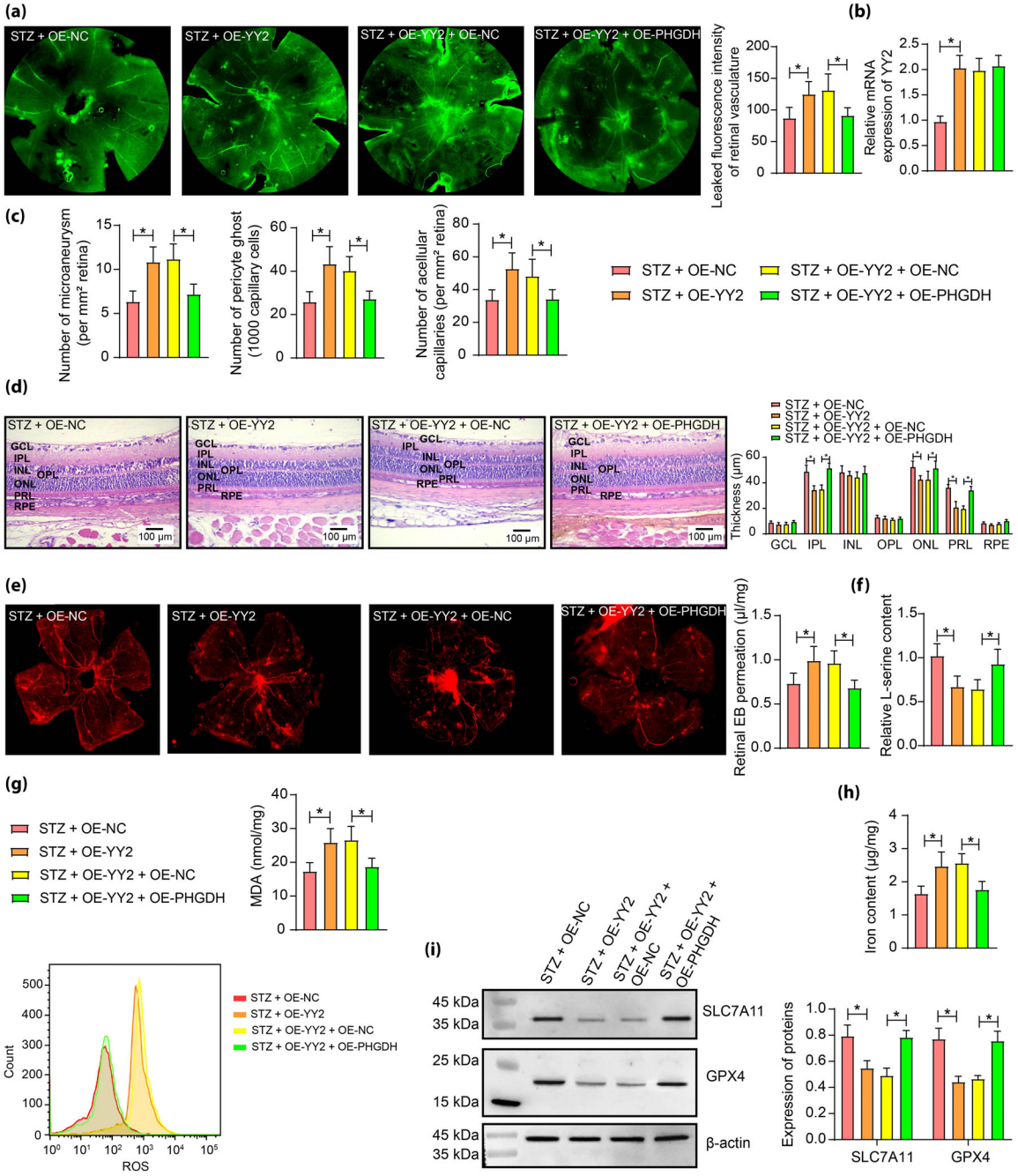

Figure 6 | The exacerbating effects of YY2 on DR in mice were mitigated by PHGDH overexpression. Mice were infected with adeno-associated virus-encapsulated overexpression PHGDH and YY2 plasmids and induced with STZ. (a) The retinal vascular changes in mice after overexpression of both YY2 and PHGDH were analyzed using FFA (n = 12). (b) The expression of YY2 in the retinal tissues of DR mice was determined using RT-qPCR (n = 6). (c) The number of pericyte ghosts, acellular capillaries, and microaneurysms in mouse retinal tissues after STZ induction was detected by trypsin digestion (n = 6). (d) Changes in retinal tissue thickness after STZ induction were observed by HE staining (n = 6). (e) Retinal vascular leakage in mice was observed using Evans blue staining (n = 6). (f) L-serine content in mouse retina in response to overexpression of both YY2 and PHGDH (n = 6). (g) Detection of the effects of overexpression of both YY2 and PHGDH on MDA and ROS content in mouse retinal tissues (n = 6). (h) Effects of overexpression of both YY2 and PHGDH on iron content in mouse retinal tissues (n = 6). (i) Effects of overexpression of both YY2 and PHGDH on the expression of ferroptosis-related proteins in mouse retinal tissues (n = 6). Data are expressed as mean ± SD. *P < 0.05. The statistical test used in (a–c, e–h) is one-way ANOVA, and in (d, i) is two-way ANOVA.

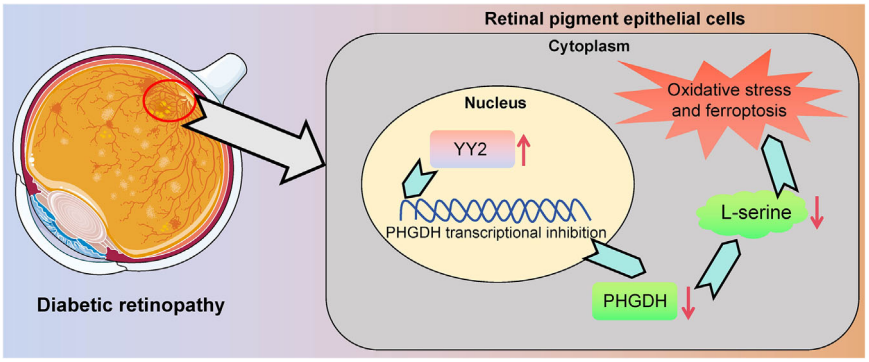

Figure 7 | Schematic diagram. The expression of YY2 was significantly elevated in diabetic retinopathy, and YY2 blocked the serine synthesis pathway in retinal epithelial cells by inhibiting the transcriptional expression of PHGDH, thereby inducing the progression of oxidative stress and ferroptosis in the cells.

Vandekeere *et al.*[20] revealed that PHGDH inhibition impaired heme synthesis, and heme deficiency induced mitochondrial respiration defects and oxidative stress in endothelial cells. Handzlik *et al.*[21] linked aberrant serine homeostasis to serine and glycine deficiencies in diabetic mice, and serine supplementation slowed neuropathy in mice. More relevantly, Eade *et al.*[22] found that functional defects in PHGDH reduced serine biosynthesis and accumulation of deoxysphingolipids in RPE cells. Furthermore, disruption of serine synthesis using CBR-5884, a specific inhibitor of PHGDH, in Müller cells aggravated oxidative damage[23]. However, whether PHGDH-mediated serine synthesis is vital for overcoming oxidative damage in PRE cells has not been explored. The pathways directly triggered by hyperglycemia play a key role in diabetic complications through the overproduction of ROS, oxidative stress, and cell death[24]. Here, our *in vitro* observations using ARPE-19 cells showed that the addition of L-serine can reduce the MDA and ROS levels and apoptosis aggravated by PHGDH knockdown. Consistently, treatment of diabetic mice with L-serine reduced protein carbonyls (3.249 ± 0.9165 nmol/mg protein) and MDA levels (1.891 ± 0.7696 μM/mg protein) in kidney tissues[25]. More relevantly, selectively knocking down PHGDH contributed to photoreceptor degeneration and decreased electroretinographic responses while supplementing exogenous L-serine protected against photoreceptor degeneration and enhanced retinal function in Müller glial cell-PHGDH knockdown mice[26].

As for the upstream modifier of PHGDH, PHGDH methylation induced by PRMT1 has been recently correlated with PHGDH activation and serine accumulation in human hepatocellular carcinoma tissues[27]. In the same vein, Yoshino *et al.*[28] revealed that PHGDH expression might be related to DNA copy number and hypomethylation in bladder cancer. Meanwhile, during senescence, PHGDH expression was reduced due to decreased levels of the transcription factor ATF4, thereby reducing intracellular serine[29]. Our bioinformatics prediction and experimental analyses demonstrated that the overexpression of YY2 was responsible for the downregulation of PHGDH in DR. Its known homology, YY1, has been reported to bind to regulatory regions of several genes specifically expressed in photoreceptors and the YY1-BS contained in the promoter of the gene encoding the final enzyme in the melatonin synthesis pathway[30]. At the cellular level, oxidative stress may result in ferroptosis, an iron-dependent form of cell death[31], while YY2 has been found to induce tumor cell ferroptosis and subsequently suppress tumorigenesis by repressing SLC7A11 transcription[32]. Therefore, we linked the YY2-controlled PHGDH transcription to oxidative stress-induced ferroptosis in DR. Ferroptosis is characterized by the GPX4 and an increase in divalent iron ions[33]. As expected, the protein expression of GPX4 and SLC7A11 was reduced in ARPE-19 cells under the exposure of HG, which was further reduced by YY2 overexpression. By contrast, PHGDH upregulation restored the expression of these two proteins *in vitro* and *in vivo*. PHGDH knockdown has been lately demonstrated to downregulate the expression of SLC7A11 through different mechanisms in different cancer cells[34, 35]. However, little is known concerning its role in controlling ferroptosis, especially under the condition of oxidative stress, which highlighted the novelty of our study.

CONCLUSIONS

In summary, our results demonstrate that oxidative stress is inhibited in DR by PHGDH overexpression, which enhances serine synthesis. In addition, overexpression of YY2 expedited RPE cells to oxidative stress-induced ferroptosis during DR via reducing the transcription of PHGDH (Figure 7). These findings open new perspectives on the relationship between PHGDH, serine synthesis, and DR, which provides a framework for additional researches regarding the mechanisms that underlie DR pathogenesis.

FUNDING
None.

DISCLOSURE
The authors declare no conflict of interest.
Approval of the research protocol: N/A.
Informed consent: N/A.
Registry and the registration no. of the study/trial: N/A.
Animal studies: All experiments were approved by the Institutional Animal Care and Use Committee of Henan Provincial People's Hospital.

DATA AVAILABILITY STATEMENT
The data that support the findings of this study are available from the corresponding author upon reasonable request.

REFERENCES
1. Lin KY, Hsih WH, Lin YB, *et al*. Update in the epidemiology, risk factors, screening, and treatment of diabetic retinopathy. *J Diabetes Investig* 2021; 12: 1322–1325.
2. Serikbaeva A, Li Y, Ma S, *et al*. Resilience to diabetic retinopathy. *Prog Retin Eye Res* 2024; 101: 101271.
3. Tan TE, Wong TY. Diabetic retinopathy: looking forward to 2030. *Front Endocrinol Lausanne* 2022; 13: 1077669.
4. Dontsov A, Ostrovsky M. Retinal pigment epithelium pigment granules: norms, age relations and pathology. *Int J Mol Sci* 2024; 25: 3609.
5. Ren J, Zhang S, Pan Y, *et al*. Diabetic retinopathy: involved cells, biomarkers, and treatments. *Front Pharmacol* 2022; 13: 953691.
6. Spillier Q, Frederick R. Phosphoglycerate dehydrogenase (PHGDH) inhibitors: a comprehensive review 2015-2020. *Expert Opin Ther Pat* 2021; 31: 597–608.
7. Okabe K, Usui I, Yaku K, *et al*. Deletion of PHGDH in adipocytes improves glucose intolerance in diet-induced obese mice. *Biochem Biophys Res Commun* 2018; 504: 309–314.
8. Zhang T, Zhu L, Madigan MC, *et al*. Human macular Muller cells rely more on serine biosynthesis to combat oxidative stress than those from the periphery. *elife* 2019; 8: e43598.
9. Wang F, Zhou H, Deng L, *et al*. Serine deficiency exacerbates inflammation and oxidative stress via microbiota-gut-brain axis in D-galactose-induced aging mice. *Mediat Inflamm* 2020; 2020: 5821428.
10. Zhou X, He L, Wu C, *et al*. Serine alleviates oxidative stress via supporting glutathione synthesis and methionine cycle in mice. *Mol Nutr Food Res* 2017; 61: 1700262.
11. Kang Q, Yang C. Oxidative stress and diabetic retinopathy: molecular mechanisms, pathogenetic role and therapeutic implications. *Redox Biol* 2020; 37: 101799.
12. Li J, Luo X, Wei M, *et al*. YY2/PHGDH axis suppresses tumorigenesis by inhibiting tumor cell de novo serine biosynthesis. *Biomed Pharmacother* 2023; 165: 115006.
13. Li L, Li Y, Timothy Sembiring Meliala I, *et al*. Biological roles of Yin Yang 2: its implications in physiological and pathological events. *J Cell Mol Med* 2020; 24: 12886–12899.
14. Fu SH, Lai MC, Zheng YY, *et al*. MiR-195 inhibits the ubiquitination and degradation of YY1 by Smurf2, and induces EMT and cell permeability of retinal pigment epithelial cells. *Cell Death Dis* 2021; 12: 708.
15. Suo L, Liu C, Zhang QY, *et al*. METTL3-mediated N(6)-methyladenosine modification governs pericyte dysfunction during diabetes-induced retinal vascular complication. *Theranostics* 2022; 12: 277–289.
16. Liao PL, Lin CH, Li CH, *et al*. Anti-inflammatory properties of shikonin contribute to improved early-stage diabetic retinopathy. *Sci Rep* 2017; 7: 44985.
17. Duraisamy AJ, Mishra M, Kowluru A, *et al*. Epigenetics and regulation of oxidative stress in diabetic retinopathy. *Invest Ophthalmol Vis Sci* 2018; 59: 4831–4840.
18. Sinclair SH, Schwartz S. Diabetic retinopathy: new concepts of screening, monitoring, and interventions. *Surv Ophthalmol* 2024; 69: 882–892.
19. Olivares AM, Althoff K, Chen GF, *et al*. Animal models of diabetic retinopathy. *Curr Diab Rep* 2017; 17: 93.
20. Vandekeere S, Dubois C, Kalucka J, *et al*. Serine synthesis via PHGDH is essential for heme production in endothelial cells. *Cell Metab* 2018; 28: 573–587 e513.
21. Handzlik MK, Gengatharan JM, Frizzi KE, *et al*. Insulin-regulated serine and lipid metabolism drive peripheral neuropathy. *Nature* 2023; 614: 118–124.
22. Eade K, Gantner ML, Hostyk JA, *et al*. Serine biosynthesis defect due to haploinsufficiency of PHGDH causes retinal disease. *Nat Metab* 2021; 3: 366–377.
23. Zhang T, Gillies MC, Madigan MC, *et al*. Disruption of de novo serine synthesis in Muller cells induced mitochondrial dysfunction and aggravated oxidative damage. *Mol Neurobiol* 2018; 55: 7025–7037.
24. Volpe CMO, Villar-Delfino PH, Dos Anjos PMF, *et al*. Cellular death, reactive oxygen species (ROS), and diabetic complications. *Cell Death Dis* 2018; 9: 119.
25. Langroudi FE, Narani MS, Kheirollahi A, *et al*. Effect of L-serine on oxidative stress markers in the kidney of streptozotocin-induced diabetic mice. *Amino Acids* 2023; 55: 799–806.
26. Shen W, Lee SR, Mathai AE, *et al*. Effect of selectively knocking down key metabolic genes in Muller glia on photoreceptor health. *Glia* 2021; 69: 1966–1986.
27. Wang K, Luo L, Fu S, *et al*. PHGDH arginine methylation by PRMT1 promotes serine synthesis and represents a therapeutic vulnerability in hepatocellular carcinoma. *Nat Commun* 2023; 14: 1011.
28. Yoshino H, Enokida H, Osako Y, *et al*. Characterization of PHGDH expression in bladder cancer: potential targeting therapy with gemcitabine/cisplatin and the contribution of promoter DNA hypomethylation. *Mol Oncol* 2020; 14: 2190–2202.

29. Wu Y, Tang L, Huang H, *et al*. Phosphoglycerate dehydrogenase activates PKM2 to phosphorylate histone H3T11 and attenuate cellular senescence. *Nat Commun* 2023; 14: 1323.
30. Bernard M, Voisin P. Photoreceptor-specific expression, light-dependent localization, and transcriptional targets of the zinc-finger protein Yin Yang 1 in the chicken retina. *J Neurochem* 2008; 105: 595–604.
31. Galaris D, Barbouti A, Pantopoulos K. Iron homeostasis and oxidative stress: an intimate relationship. *Biochim Biophys Acta Mol Cell Res* 2019; 1866: 118535.
32. Li Y, Li J, Li Z, *et al*. Homeostasis imbalance of YY2 and YY1 promotes tumor growth by manipulating ferroptosis. *Adv Sci (Weinh)* 2022; 9: e2104836.
33. He W, Chang L, Li X, *et al*. Research progress on the mechanism of ferroptosis and its role in diabetic retinopathy. *Front Endocrinol Lausanne* 2023; 14: 1155296.
34. Shen L, Zhang J, Zheng Z, *et al*. PHGDH inhibits ferroptosis and promotes malignant progression by upregulating SLC7A11 in bladder cancer. *Int J Biol Sci* 2022; 18: 5459–5474.
35. Wang J, Zeng L, Wu N, *et al*. Inhibition of phosphoglycerate dehydrogenase induces ferroptosis and overcomes enzalutamide resistance in castration-resistant prostate cancer cells. *Drug Resist Updat* 2023; 70: 100985.

SUPPORTING INFORMATION

Additional supporting information may be found online in the Supporting Information section at the end of the article.

Figure S1 | The potential regulatory capacity of YY2 for PHGDH.